Hindawi Publishing Corporation
International Journal of Antennas and Propagation
Volume 2012, Article ID 378798, 8 pages
doi:10.1155/2012/378798

Research Article

Single Feed Aperture-Coupled Wideband Dielectric Resonator Antenna with Circular Polarization for Ku-Band Applications

Joshua M. Patin and Satish K. Sharma

Department of Electrical and Computer Engineering, San Diego State University, 5500 Campanile Drive, San Diego, CA 92182-1309, USA

Correspondence should be addressed to Satish K. Sharma, ssharma@mail.sdsu.edu

Received 17 March 2012; Revised 29 April 2012; Accepted 1 May 2012

Academic Editor: Hon Tat Hui

A novel single feed aperture-coupled wideband dielectric resonator antenna (DRA) exhibiting righ-handed circular polarization (RHCP) operating in the Ku-band frequency range is presented. The aperture-coupled single feed design utilizes back-side microstrip excitation through a novel bow-tie-shaped cross-slots in the ground plane. Extensive simulation parametric studies resulted in a 3 dB axial ratio (AR) bandwidth of 17.24% at a center frequency of 13 GHz, where the dielectric resonator is excited in its $HEM_{11\delta}$ resonant mode. A prototype DRA was fabricated with some limitations and experimentally verified for the impedance matching and radiation patterns showing circular polarization.

1. Introduction

Dielectric resonator antennas (DRAs) were first discovered in 1983 by Long et al., and since then they have been widely studied [1]. Their inherent features of high radiation efficiency, ease of excitation, compactness, and ability to obtain radiation patterns using different excitation modes offer much to an antenna application [2]. Furthermore, the shape of a DRA can be custom, resulting in favorable operating modes or polarizations. The DRAs supporting circular polarizations have been studied and can be found in the literature. Traditionally, circular polarization is achieved using quadrature couplers and elaborate feed systems which can also be done with DRAs as well [3, 4]. The design in [4] is unique in using a dual mode dielectric resonator (DR) excited by vertical strips fed in quadrature, while [3] uses an underlaid hybrid coupler. Furthermore, four DRA arrays can be excited using sequential rotation to obtain wide axial ratio bandwidths [5].

Single feed excited DRAs providing circular polarization are typically more desirable due to their simple geometry and are also more challenging to obtain wide axial ratio bandwidths. A half cylinder circular sector DRA on a ground plane was demonstrated to provide single feed circular polarization 3 dB axial ratio (AR) bandwidth of 10% [6]. This design uses tuned probe feed placement which excites the two spatially orthogonal modes in quadrature phase to achieve the circular polarization. Another more recent design utilizes a complex configuration of an upside-down rectangular stair-shaped DRA excited by a microstrip through a rotated 45° slot to achieve circular polarization [7]. This design was able to achieve 10.6% 3 dB AR bandwidth; however, it requires a complex DRA shape and precise registration of the DRA with respect to the slot in order to achieve the performance.

One common method for achieving the spatially orthogonal modes for circular polarization is to use crossed slots in the ground plane excited by a microstrip transmission line. In this configuration, the crossed slots are at 90° with respect to (w.r.t.) each other and are both at 45° w.r.t. the back-side microstrip line. An optimization of this topology was presented in [1], where offsetting each slot from the end of the microstrip line (thereby having the slot's intersection off from DR center) allows for AR bandwidths up to 4.7% at broadside angle ($\theta = 0°$). This design excites the fundamental $HEM_{11\delta}$ mode at 5.7 GHz, where the lengths of slots and distance of slots to the end of the microstrip

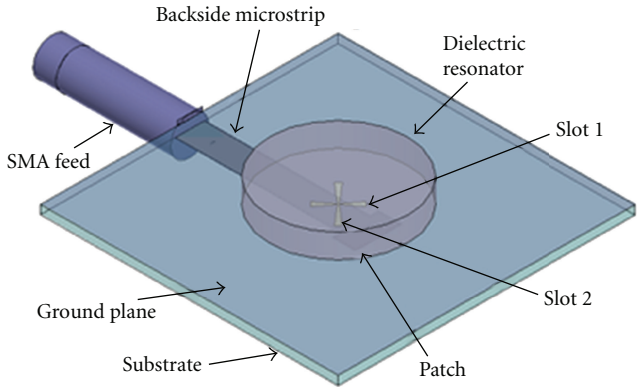

Figure 1: Geometry of the DRA displaying various components.

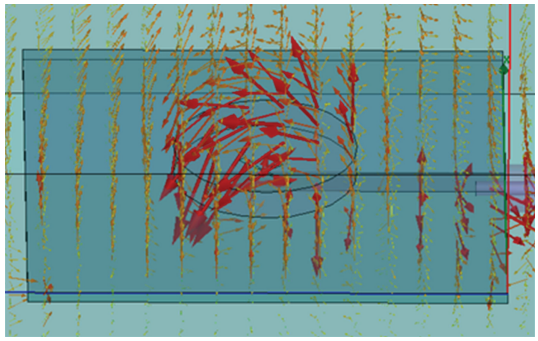

Figure 2: E-Field vectors showing $HEM_{11\delta}$ mode of DRA.

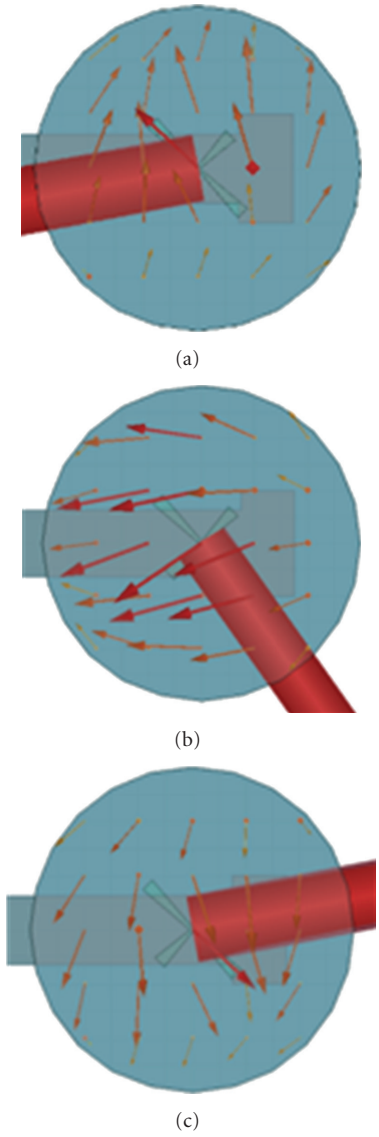

Figure 3: E-Fields rotating from 0° (a), to 90° (b), to 180° (c), showing mechanism of RHCP operation.

line are tuned for the optimized performance. In [8], a trapezoidal DRA is presented which offers wideband circular polarization performance. In [9], simulated results on a dual band single feed excited cylindrical DRA are discussed which provides both linear and circular polarizations. However, in this paper, investigation results on a single feed excited single wideband cylindrical DRA is presented which further enhances the design concept in [1] by using a novel bow-tie-shaped slot to increase the AR bandwidth to 17.24% at Ku-band frequencies.

2. DRA Geometry

The aperture-coupled excited DRA through the bow-tie cross-slots was designed and simulated using Ansoft's High Frequency Structural Simulator (HFSS) and is shown in Figure 1. The DRA consists of an end-launched SMA excited by a 50Ω microstrip transmission line with stub on the backside of a low-loss substrate (Rogers Duroid 5880, ε_r = 2.20), the bow-tie cross-slots in the ground plane, and the DR on top of the slots. The dimensions of the cross-slots, the DR, and the ground plane determining the antenna performance are labeled in Figure 1. The slot widths at the center of the bow-tie and the ends of the slots are 0.1 mm and 0.5 mm, respectively, with the length of slot 1 and slot 2 being 3.4 mm and 4.65 mm, respectively. The slots are centered with each other and with the DR in the ground plane and substrate. The substrate is 33 mm × 33 mm, 32 mil (0.7874 mm) thick, and is made out of Rogers Duroid 5880TM (ε_r = 2.20). The backside of the substrate has a 50Ω microstrip transmission line with a small stub of 2 mm × 4 mm at the end which aids in the impedance matching. The DR is made out of Rogers TMM10 material (ε_r = 9.20). The resonator is cylindrical with a radius of 6 mm and a height of 2.12 mm.

The DR is excited in the fundamental $HEM_{11\delta}$ mode. The E-Field vectors clearly displaying the excited $HEM_{11\delta}$ mode are shown in Figure 2. In the configuration shown in Figure 1, the antenna has right hand circular polarization (RHCP) since slot 2 is longer than slot 1. The RHCP operation of the DRA is clearly illustrated in Figures 3(a)–3(c), where the field rotates circularly with phase.

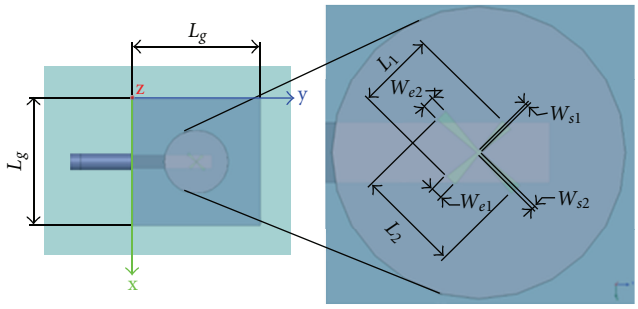

FIGURE 4: DRA with labels showing important design parameters.

3. Simulated DRA Performance

3.1. Parametric Studies. Extensive parametric studies were conducted on an early variant of the final design in order to understand how best to tune for wide axial ratio (AR) bandwidth, and impedance matching. Although this study incorporated eight parameters, the most prominent and useful were the cross-slot lengths L_1 and L_2, the slot start widths W_{S1} and W_{S2}, slot end widths W_{e1} and W_{e2}. These parameters are shown graphically in Figure 4 for clarity.

3.1.1. Slot Lengths. The DRA is excited from the backside microstrip line, through the bow-tie cross-slots, where their physical dimensions play a critical role in proper DRA excitation. The slots were modified one at a time to isolate each slot's effect on the antenna performance. L_1 was swept from 3.13 mm to 3.53 mm in 0.1 mm steps, while L_2 was swept from 4.24 mm to 4.64 mm in 0.1 mm increments.

The length of slot 1, L_1, has a pronounced effect on both impedance match (S_{11}) and axial ratio versus frequency, as shown in Figures 5(a) and 5(b). Due to its shorter length, L_1 dominates the higher frequency resonance seen in the impedance match (S_{11}) plot of Figure 5(a). As L_1 is increased, the CP performance moves down in frequency, while spanning a smaller frequency band, and the input impedance is better matched at the lower frequencies under this condition. As the length is decreased, there is a point where optimal axial ratio bandwidth is achieved as the two resonances of the antenna even out giving the largest bandwidth. The antenna loses matching at the lower frequency band while the upper part of the impedance match moves up in frequency.

The length of slot 2, L_2, does not exhibit the same controlled characteristics over the antenna's AR performance. As shown in Figures 6(a) and 6(b), as L_2 is decreased, the antenna impedance match improves, but the AR performance is degraded. The variation of AR is not as great as from varying L_1. Due to its larger size, L_2 dominates the lower frequency resonance in this design.

3.1.2. Slot Start Widths. Next, the bow-tie slot's starting widths, W_{S1} and W_{S2} , were swept independently from 0 mm to 0.2 mm in 0.05 mm increments. While one slot was modified, the other was set at 0.1 mm. The results from this study are summarized in Figures 7(a) and 7(b) for W_{S1} and Figures 8(a) and 8(b) for W_{S2}. The results from this study are similar to the slot length study conducted earlier. From Figures 7(a) and 8(a), it is apparent that modifying slot 1 affects the upper resonance and slot 2 affects the lower resonance. An interesting note here is that increasing W_{S1} causes the resonance in S_{11} to move up in frequency. Increasing W_{S2} causes the lower resonance to become more

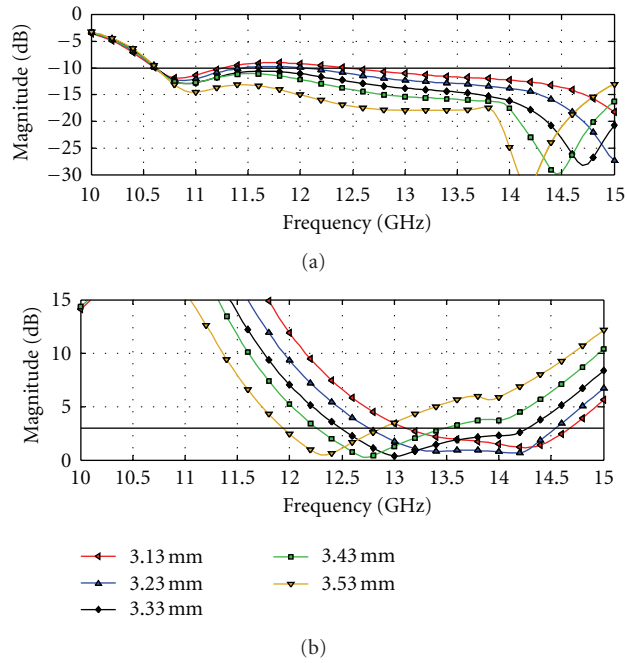

FIGURE 5: (a) Reflection coefficient magnitude (S_{11}), and (b) axial ratio versus frequency for variation of L_1, slot 1 length.

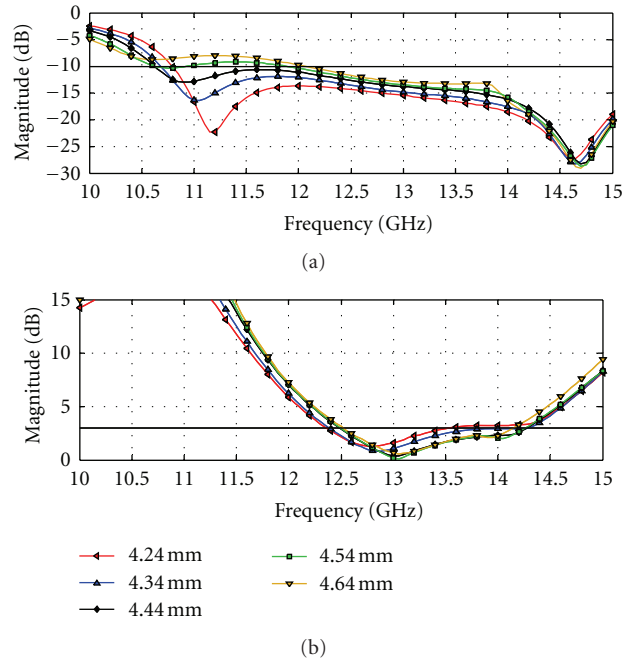

FIGURE 6: (a) Reflection coefficient magnitude (S_{11}), and (b) axial ratio versus frequency for variation of L_2, slot 2 length.

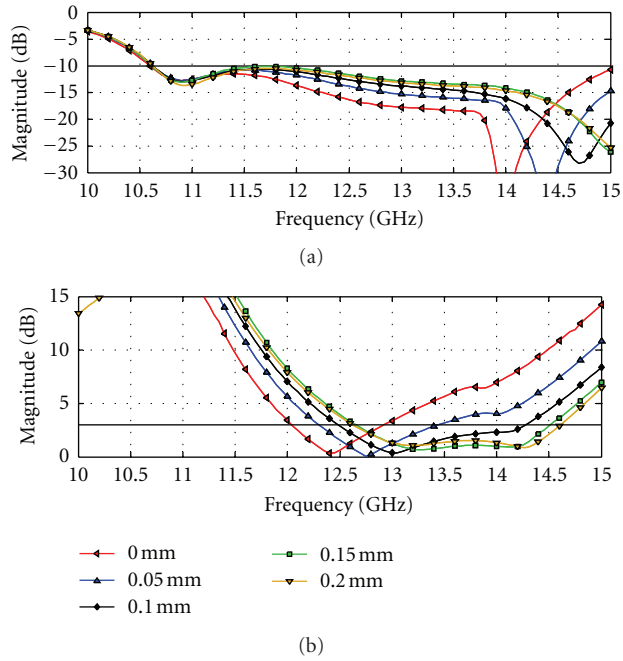

FIGURE 7: (a) Reflection coefficient magnitude (S_{11}), and (b) axial ratio versus frequency for variation of W_{S1}, slot 1 start width.

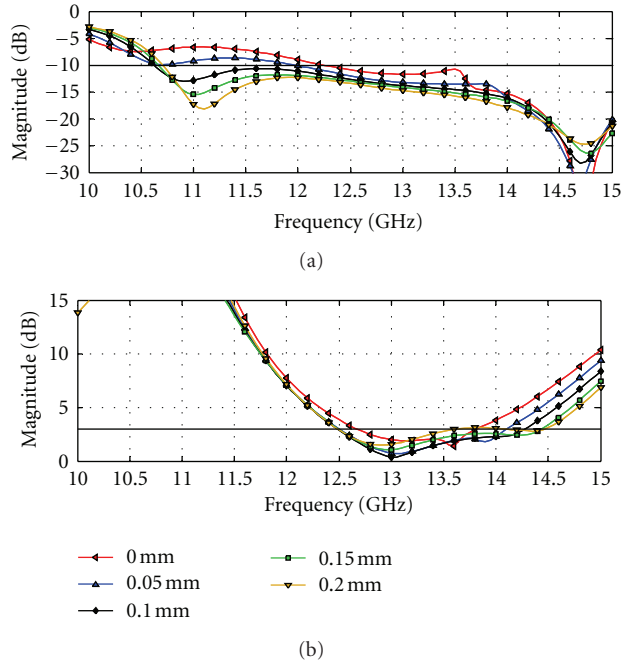

FIGURE 8: (a) Reflection coefficient magnitude (S_{11}), and (b) axial ratio versus frequency for variation of W_{S2}, slot 2 start width.

pronounced, improving match, while axial ratio (AR) suffers. In this study, variation on W_{S2} does not have the same magnitude of effect on the AR and impedance matching as W_{S1}, showing that the geometry of W_{S1} dominates these parameters.

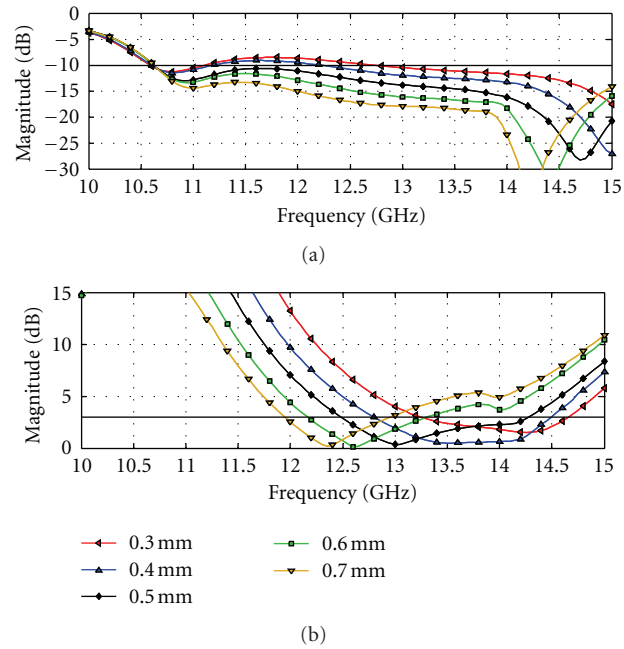

FIGURE 9: (a) Reflection coefficient magnitude (S_{11}), and (b) axial ratio versus frequency for variation of W_{e1}, slot 1 end width.

3.1.3. Slot End Widths. In this study, the bow-tie slot's ending widths, W_{e1} and W_{e2}, were swept independently from each other to discover their effects on the design. The results of this study were similar to the slot length and slot start widths in that slot 1 dominates the impedance matching and AR performance. Figures 9(a) and 9(b) display the impedance matching and AR performance versus frequency for W_{e1}, and Figures 10(a) and 10(b) display the impedance matching and AR performance versus frequency for W_{e2}. Figures 9(a) and 9(b) show that as W_{e1} is increased, the higher frequency resonance is affected most, decreasing in frequency and narrowing the impedance bandwidth. Impedance matching bandwidth and AR bandwidth performance also decrease in frequency. A value of 0.4 mm seems to have the most symmetrical and flattest AR response, centered around 13.75 GHz, but 0.5 mm actually provides a larger AR bandwidth. As with previously discussed studies, slot 2 dominates the lower frequency resonance and has less of a pronounced impact on impedance matching and axial ratio (AR). Figures 10(a) and 10(b) show the response for W_{e2} for impedance match and AR bandwidths. As W_{e2} is decreased, the lower resonance becomes more defined and impedance match improves, but AR performance slightly worsens.

3.2. Final Design. The desired center frequency of operation for the DRA is 13 GHz. The parametric studies indicated that the operating frequency was closer to 13.75 GHz. This was accomplished by modifying the DR, slots, and ground plane. The DR was changed from a cylinder of radius 6.22 mm and height of 2 mm to a cylinder of radius 6 mm and height of 2.12 mm. The slot dimensions were increased from 3.33 mm to 3.4 mm for slot 1, and 4.44 mm to 4.65 mm for slot 2. The

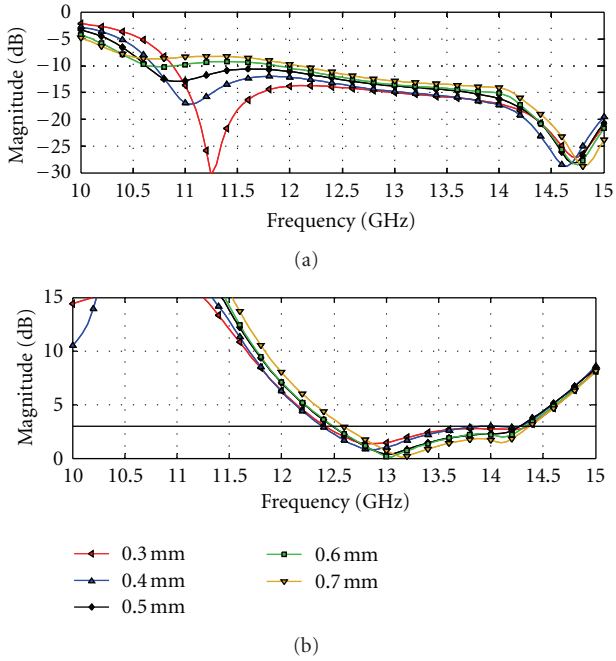

FIGURE 10: (a) Reflection coefficient magnitude (S_{11}), and (b) axial ratio versus frequency for variation of W_{e2}, slot 2 end width.

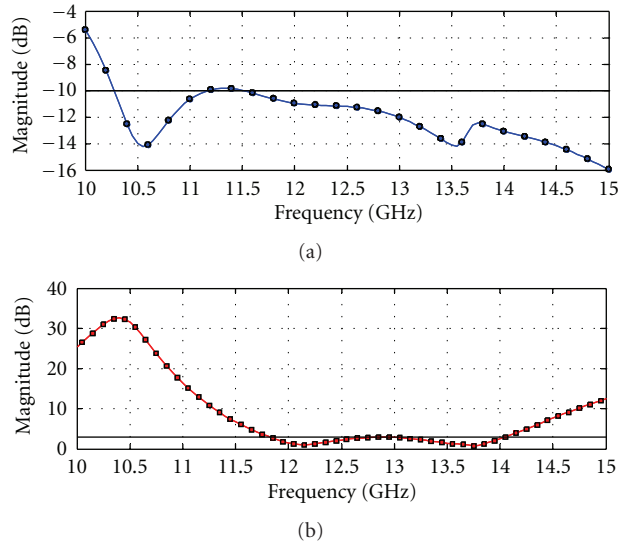

FIGURE 11: (a) Reflection coefficient magnitude (S_{11}), and (b) axial ratio versus frequency for simulated final DRA design.

ground plane was increased from 25 mm square to 33 mm square. A 2 mm × 4 mm stub was added to the end of the microstrip line to aid in matching. These changes were driven heavily by the parametric studies and resulted in a 13 GHz center frequency, 17.24% 3 dB axial ratio (AR) bandwidth, and 35.3% largest continuous impedance bandwidth.

3.2.1. Impedance and Axial Ratio Bandwidths. The DRA achieves acceptable impedance matching, axial ratios, and gain for the RHCP band. The S_{11} plot for the antenna is shown in Figure 11(a), and the AR plot is shown in Figure 11(b). Figure 11(a) shows the −10 dB matching to be in two areas, from 10.28 GHz to 11.15 GHz (8.1%), and then from 11.5 GHz to 16.48 GHz (35.3%). Attempts to match the entire band resulted in degraded antenna performance on other metrics, such as axial ratio bandwidth and gain. Figure 11(b) illustrates the AR over frequency, where AR is computed at $\theta = 0°$. This plot shows the CP region spanning from 11.82 GHz to 14.05 GHz, defined by less than 3 dB AR, which accounts to 17.2% fractional bandwidth while impedance matched better than $S_{11} = -10$ dB.

3.2.2. Gain and Efficiency. The radiation efficiency versus frequency for the DRA is shown in Figure 12(a), where the RHCP band exhibits radiation efficiencies ranging from 96.2% to 97.4%. The gain versus frequency plot in Figure 12(b) displays positive gain (dBic) throughout the RHCP band. Clearly the RHCP and LHCP gain plots show how the antenna changes from being almost linearly polarized around 10.55 GHz with both RHCP and LHCP being nearly equal, to RHCP at 13 GHz as the LHCP gain degrades to below −10 dBic.

3.2.3. Radiation Pattern Performance. The radiation patterns were studied over the frequency bandwidth of interest and are shown in Figures 13(a)–13(c) at 12 GHz, 13 GHz, and 14 GHz within the bandwidth, respectively. At 12 GHz, the bottom of the CP band, the DRA exhibits a 3 dB beamwidth of 105.5° with an 11.4 dB front-to-back (F/B) ratio. The maximum gain found at $\theta = 0°$ is 4.16 dBic. At 13 GHz, the center of the CP band, the DRA exhibits a 3 dB beamwidth of 117° with a front-to-back (F/B) ratio of 17.4 dB. The maximum gain found at $\theta = 0°$ is 4.7 dBic. Similarly, at 14 GHz, the top of the RHCP band, the 3 dB beamwidth is 134.5° with a 15.45 dB front-to-back (F/B) ratio. The maximum gain found at $\theta = 0°$ is 3.82 dBic, which is somewhat lower than the other two frequencies in this band because cross-polarization LHCP component is slightly higher than other two frequencies.

4. Experimental Verifications

The antenna was challenging to fabricate due to its small size and high frequency, making it sensitive to physical variations from the simulated design. A best attempt was made at milling the Rogers TMM10 dielectric material of thickness 2.54 mm for achieving the DR with height of 2.12 mm, while an LPKF milling machine was used to route the substrate and microstrip transmission line from the Rogers Duroid 5880TM including the bow-tie cross-slots. The next challenge was in aligning the DR on top of the cross-slots, which was done by drawing cross points, both on the DR and cross-slots using a fine point marker pen. The DR was glued using regular permanent glue with unknown electrical properties. However, it seems some misalignment appeared in doing so, which appears difficult to fix manually at Ku-band frequency (13 GHz). Photographs of the fabricated prototype antenna is shown in Figures 14(a) and 14(b) for the top and bottom views of the antenna, respectively.

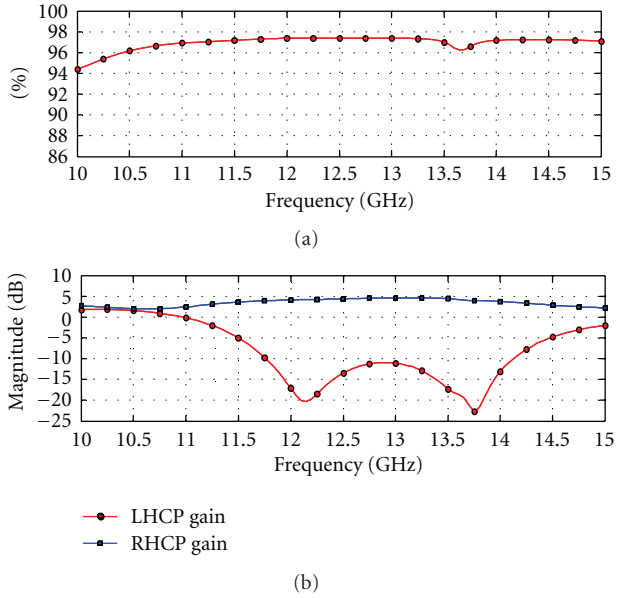

Figure 12: Radiation efficiency (a) and CP gain (b) versus frequency.

The fabricated antenna performance is shown in Figures 15 and 16. The impedance plot in Figure 15 illustrates the measured versus simulated reflection coefficient magnitude (S_{11}) performance for the DRA. It is clear that some matching is obtained close to the band of interest, but some variation exists especially in the higher frequency above 13.5 GHz. From Figure 15, the fabricated antenna appears to be shifted down in frequency by nearly 1 GHz from the simulation result. In addition, frequencies between 11.5 GHz and 12.5 GHz are showing matching level approaching $S_{11} = -9$ dB, which can be attributed to the fabrication errors.

Figures 16(a)–16(c) show radiation patterns at 11.5 GHz, 12 GHz, and 12.5 GHz, respectively. The radiation pattern measurements were made using a continuously rotating linear polarized Satimo broadband horn calibrated for the band of operation in the Antenna and Microwave Laboratory (AML) at San Diego State University. These measurements show acceptable circular polarized (CP) patterns with axial ratio within 3 dB limit at the broadside angle. Further, it confirms the operation of the fabricated antenna at a lower frequency than the expected simulated frequencies which are attributed to the fabrication errors.

5. Conclusions

An aperture-coupled RHCP DRA operating in Ku-band has been presented which is driven from a single feed and excited through a novel bow-tie cross-slots. Extensive parametric studies were conducted which identified important tuning parameters aside from the standard DR dimension sensitivities. The DRA was then tuned for 13 GHz center frequency operation providing a 3 dB axial ratio (AR) bandwidth of 17.24% while −10 dB matching criteria are met. The simulated radiation patterns show acceptable

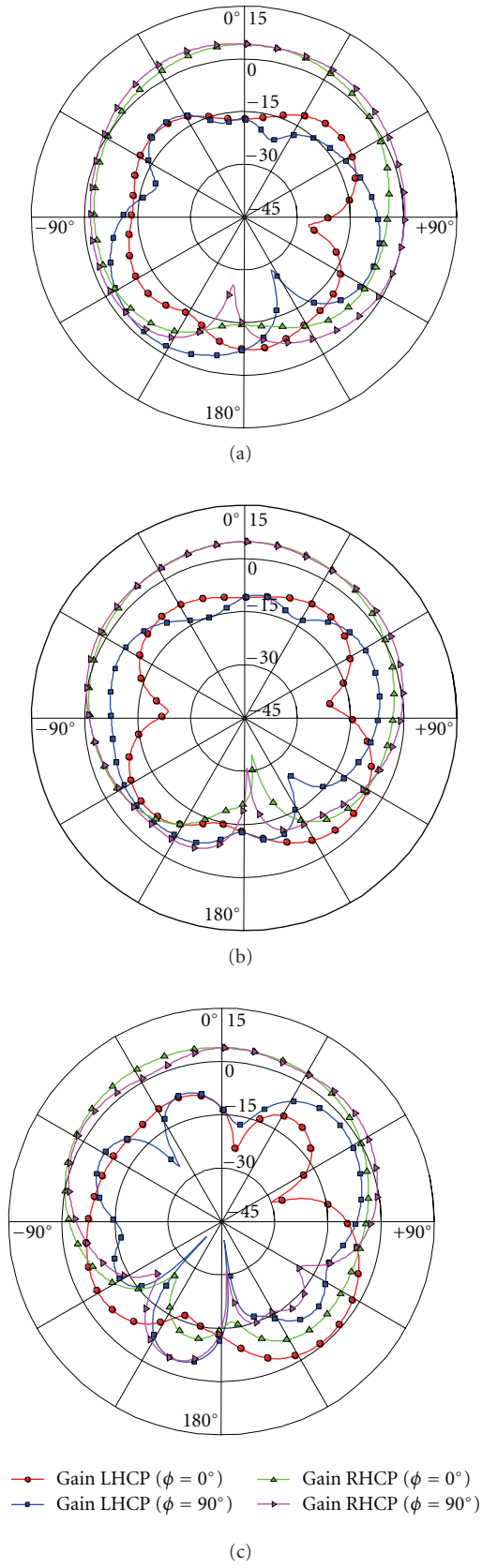

Figure 13: RHPC radiation pattern for (a) 12 GHz, (b) 13 GHz, and (c) 14 GHz.

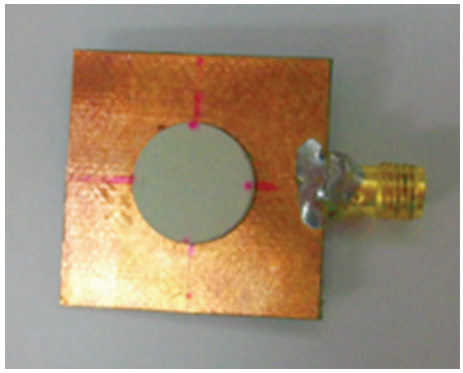

(a)

(b)

Figure 14: Photographs of the fabricated D showing top and bottom views.

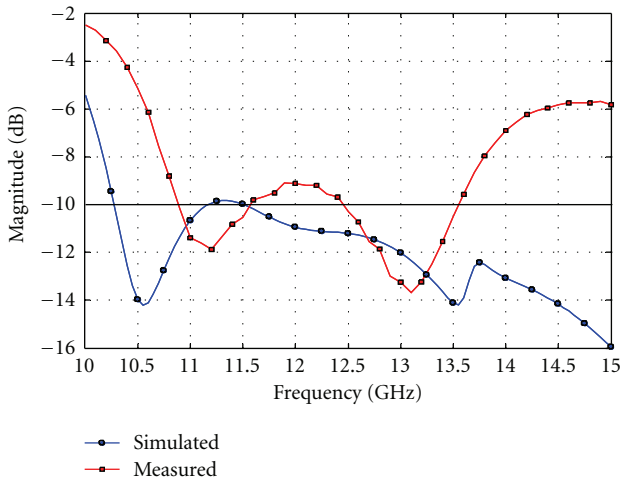

Figure 15: Simulated and measured reflection coefficient magnitudes (S_{11}).

co- and crosspolarization separation over the AR band. The DRA was fabricated and tested using rotating linear polarization method. The fabricated DRA exhibited operation centered around 12 GHz, with acceptable circularly polarized radiation patterns. The difference in simulated and measured performance of the antenna is primarily attributed to manufacturing errors of the DR and its misalignment on

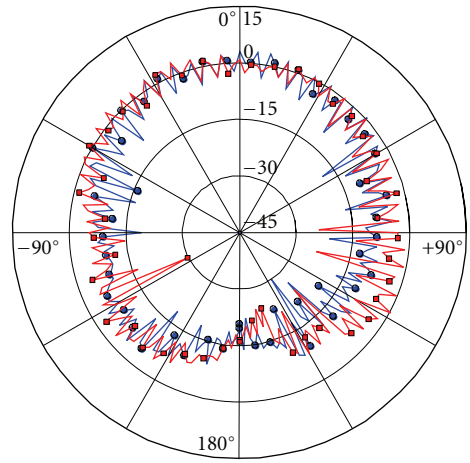

(a)

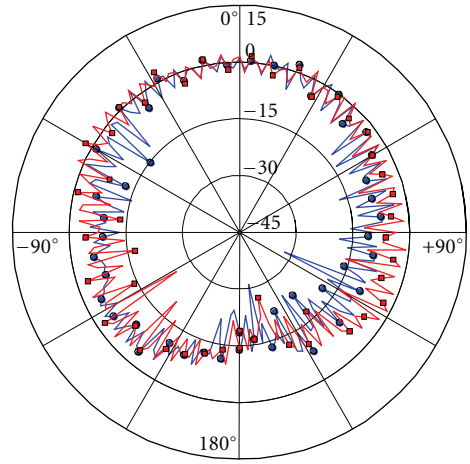

(b)

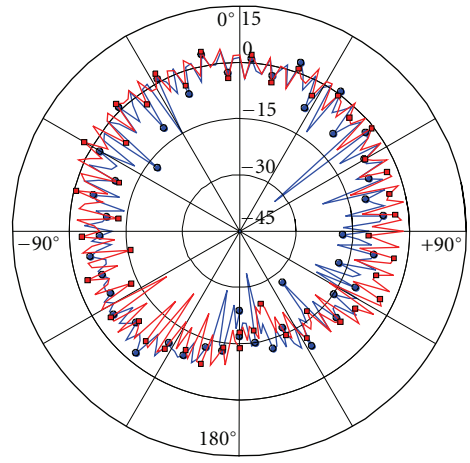

(c)

Figure 16: Radiation pattern for the fabricated DRA at (a) 11.5 GHz, (b) 12 GHz, and (c) 12.5 GHz.

the cross-slots. This DRA can find applications in Ku-band-based satellite communication applications.

Acknowledgment

One of the authors (J. M. Patin) would also like to thank B. Shanmugam for his help in fabrication and measurement of the antenna. The work was supported in part by National Science Foundation (NSF) under CAREER Grant no. ECCS-0845822.

References

[1] G. Almpanis, C. Fumeaux, and R. Vahldieck, "Offset cross-slot-coupled dielectric resonator antenna for circular polarization," *IEEE Microwave and Wireless Components Letters*, vol. 16, no. 8, pp. 461–463, 2006.

[2] S. A. Malekabadi and S. M. Moghadasi, "Circular polarized rectangular dielectric resonator antenna using single probe feeds," in *Proceedings of the 12th International Conference on Mathematical Methods in Electromagnetic Theory (MMET '08)*, vol. 16 of *IEEE Microwave and Wireless Components Letters*, pp. 199–201, July 2008.

[3] E. H. Lim, K. W. Leung, and X. S. Fang, "The compact circularly-polarized hollow rectangular dielectric resonator antenna with an underlaid quadrature coupler," *IEEE Transactions on Antennas and Propagation*, vol. 59, no. 1, pp. 288–293, 2011.

[4] B. Li, C. X. Hao, and X. Q. Sheng, "A dual-mode quadrature-fed wideband circularly polarized dielectric resonator antenna," *IEEE Antennas and Wireless Propagation Letters*, vol. 8, pp. 1036–1038, 2009.

[5] S. L. S. Yang, R. Chair, A. A. Kishk, K. F. Lee, and K. M. Luk, "Circular polarized elliptical dielectric resonator antenna sub array fed by hybrid-ring feeding network," in *IEEE Antennas and Propagation Society International Symposium (APS '06)*, pp. 2221–2224, July 2006.

[6] M. T. K. Tarn and R. D. Murch, "Circularly polarized circular sector dielectric resonator antenna," *IEEE Transactions on Antennas and Propagation*, vol. 48, no. 1, pp. 126–128, 2000.

[7] R. Chair, S. L. S. Yang, A. A. Kishk, K. F. Lee, and K. M. Luk, "Aperture fed wideband circularly polarized rectangular stair shaped dielectric resonator antenna," *IEEE Transactions on Antennas and Propagation*, vol. 54, no. 4, pp. 1350–1352, 2006.

[8] Y. Pan and K. W. Leung, "Wideband circularly polarized trapezoidal dielectric resonator antenna," *IEEE Antennas and Wireless Propagation Letters*, vol. 9, pp. 588–591, 2010.

[9] J. Patin and S. K. Sharma, "Dual band single feed dielectric resonator antenna with linear and circular polarizations for Ku-band," in *Proceedings of the IEEE International Symposium on Antennas and Propagation*, 2011.